ACS NANO

www.acsnano.org

ARTICLE

Nanotransfer Printing on Textile Substrate with Water-Soluble Polymer Nanotemplate

Jiwoo Ko, Zhi-Jun Zhao, Soon Hyoung Hwang, Hyeok-Joong Kang, Junseong Ahn, Sohee Jeon, Moonjeong Bok, Yongrok Jeong, Kyungnam Kang, Incheol Cho, Jun-Ho Jeong,* and Inkyu Park*

Cite This: *ACS Nano* 2020, 14, 2191−2201

Read Online

ACCESS | Metrics & More | Article Recommendations | Supporting Information

ABSTRACT: The growing interest in wearable devices has drawn increased attention to smart textiles, and various transfer methods have therefore been introduced to realize the desired functions using textiles as substrates. However, the existing transfer techniques are not suited for the production of sophisticated nanoscale patterns on textiles, as textile roughness and difficulty of precise pattern size control hinder miniaturization, deteriorate device performance, and complicate the use of optical phenomena such as surface plasmon resonance. To address these limitations, we have developed a method based on simple dissolution of a water-soluble nanopatterned polymer film for the facile transfer of nanostructures of on-film-deposited functional materials onto textile substrates. The above method tolerates a variety of functional materials, e.g., metals and SiO_2, and nano/microscale structures, e.g., nanoscale lines, dots, holes, and mesh patterns with a minimum pattern width of 50 nm. The proposed technique is employed to fabricate a palladium nanoscale line array (utilized as a highly sensitive and selective hydrogen sensor) and is shown to be suitable for the production of security patterns on textiles, as it allows the printing of complex nanostructure patterns with electrical and optical functionalities.

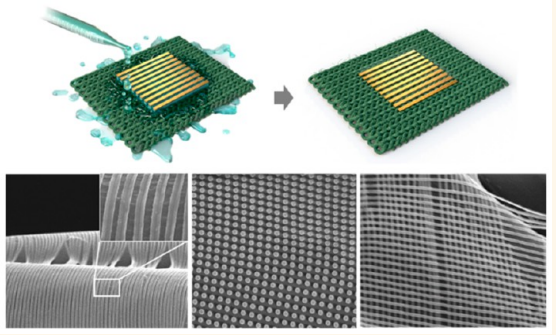

KEYWORDS: *smart textile, nanotransfer printing, water-soluble polymer, gas sensor, nanostructure*

With the development of flexible and wearable electronics,[1] smart textiles have been used in various applications such as physical sensors,[2−11] chemical sensors,[12−19] optical devices,[8,20] and generators/energy storage.[5,21−30] Recently, researchers have developed functional devices based on smart textiles using various fabrication methods including weaving fibers in desired patterns,[2,4,7−10,20,31−36] spray coating through screen masks,[37] dip coating,[3,38] and inkjet printing.[18] However, these methods cannot produce fine nanoscale patterns that are essential for miniaturized sensors, displays, energy harvesting devices, and various wearable electronic devices requiring high performance and high device integration density. Among these fabrication methods, the interweaving of functional fibers allows for high durability on the textile substrate but suffers from limited downscaling because unit patterns (i.e., knot and weave) are in the millimeter scale. Spray and dip coating methods are simple, but micro/nanoscale patterns cannot be produced because of undesirable excessive ink spreading on the textile during the coating process. In the case of inkjet printing, the patterning of structures down to tens of micrometers is relatively easier than weaving and coating methods, but nanoscale patterning cannot be achieved. In other words, all aforementioned methods are not suitable for achieving the desired patterns at the nanoscale. Therefore, to overcome the limitations of current fabrication methods, an alternative process that can realize the desired patterns of functional materials at the nanoscale on textile substrates should be developed. It was determined that the transfer printing method could address these technical challenges. The conventional transfer process is realized by the following sequential steps: (1) micro/nanopatterning on a donor substrate and (2) transfer of patterns on the receiver substrate.[39,40] Transfer printing has been developed and utilized for the fabrication of various functional devices such as flexible electronic devices,[41] sensors,[42] energy harvesting devices,[43,44] and display devices.[45] However, conventional transfer printing methods have strict requirements for the surface morphologies and roughness of receiver substrates. Therefore, conventional transfer printing methods cannot be directly used for the fabrication of nanostructures on textile

Received: November 15, 2019
Accepted: January 28, 2020
Published: January 28, 2020

https://dx.doi.org/10.1021/acsnano.9b09082
ACS Nano 2020, 14, 2191−2201

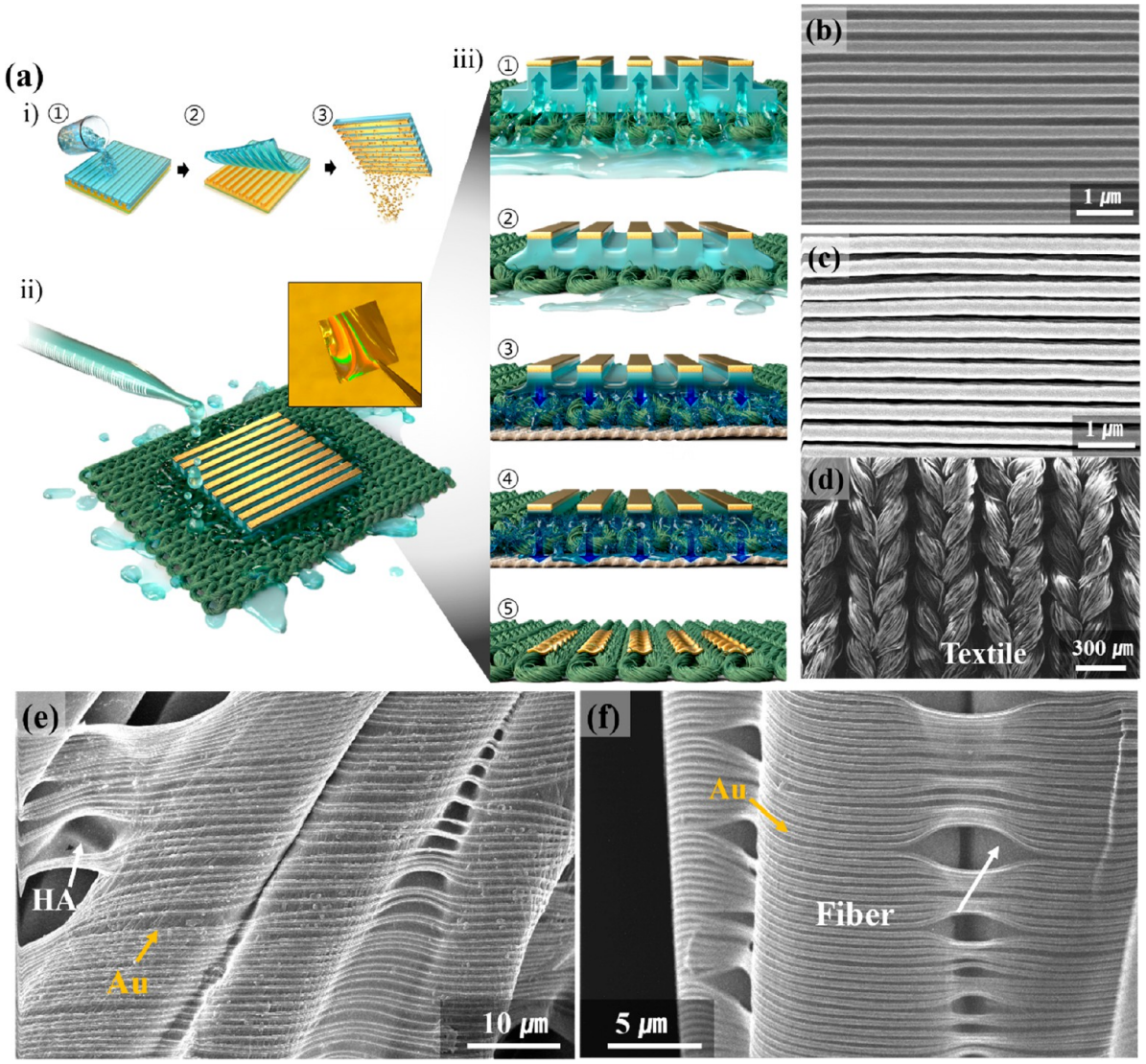

Figure 1. nTP-SP of functional materials: (a) nTP-SP mechanism and fabrication process, (b) SEM image of an HA film with a line width and spacing (L/S) of 200 nm/200 nm, (c) SEM image of obliquely deposited Au on a HA film having L/S of 200 nm/200 nm, (d) SEM image of the original textile, (e) SEM image of transferred Au patterns when HA is not completely dissolved, and (f) SEM image of transferred Au patterns after completely removing HA from the fibers.

substrates. To apply this process to textile substrates with rough surface morphologies, careful modification of the process parameters such as the transfer process environment and donor substrate material is required. In the nanotransfer printing (nTP) process proposed in this study, the wetting property of the textile was exploited, and nanostructures of functional materials could be transferred using a water-soluble donor substrate with nanoscale patterns. By dissolving the donor substrate, the functional nanostructures deposited on the donor substrate were transferred on the rough surface of the textile substrate.

Herein, hyaluronic acid (HA) was used as the donor substrate because it is a biocompatible polymer with good water solubility at room temperature. Moreover, it could easily replicate the nanostructures by a molding process on the Si master. First, a HA mold with a designed nanostructure pattern (i.e., nanoscale lines, dots, and holes) was prepared from a polymer mold. Second, various metals or SiO_2 were deposited on the patterned HA film. Finally, when the film was placed on a wet textile substrate, it dissolved, and the designed nanostructures of functional materials were transferred onto the textile. Using this process, metal or nonmetal micro/nanoscale patterns could be transferred onto the nonflat surface of the textile while retaining their shapes. A Pd line array gas sensor was successfully fabricated on a textile using this proposed method. Furthermore, security patterns could be implemented by exploiting the optical and electronic properties of the transferred nanoscale patterns.

RESULTS AND DISCUSSION

The nanotransfer printing process using water-soluble polymer (nTP-SP) and the corresponding morphologies of the nanostructures fabricated on textiles are shown in Figure 1. The prepared HA solution is first poured on the polymer mold with designed nanostructures (Figure 1a(i-1)), and the HA film with nanostructures is then separated from the polymer mold (Figure 1a(i-2)). The corresponding scanning electron microscopy (SEM) image is shown in Figure 1b. Next, the functional material is obliquely deposited on the fabricated HA film *via* electron beam evaporation (Figure 1a(i-3)).[46] The

https://dx.doi.org/10.1021/acsnano.9b09082
ACS Nano 2020, 14, 2191−2201

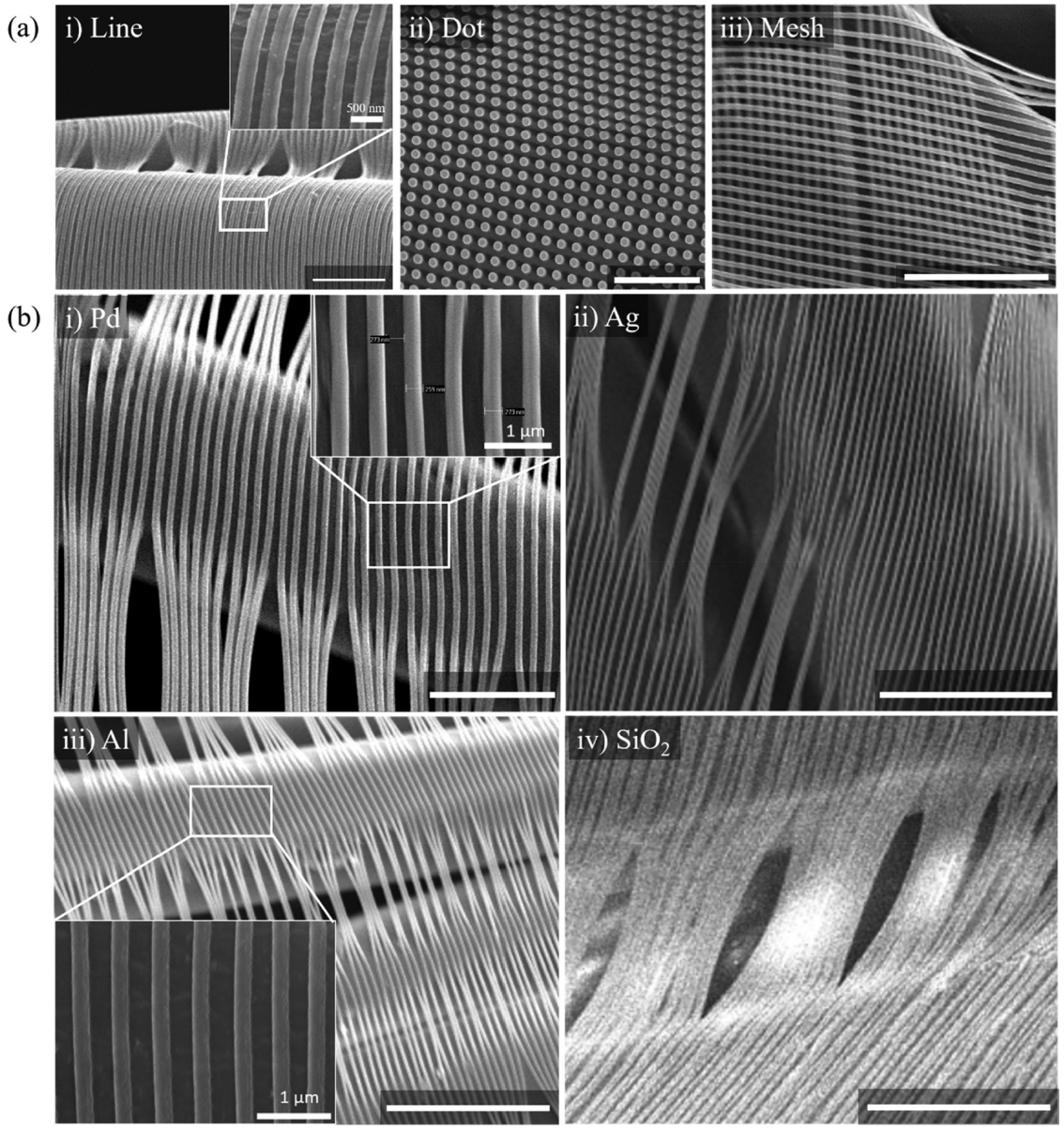

Figure 2. SEM images of various transferred nanopatterns and functional materials: (a) Au nanopatterns including (i) line array with L/S of 200 nm/200 nm, (ii) dot array with a diameter of 480 nm and a pitch of 1000 nm, and (iii) mesh with L/S of 200 nm/200 nm; (b) transferred nanopatterns of various other materials such as (i) Pd nanoscale line array with L/S of 200 nm/200 nm, (ii) Ag nanoscale line array with L/S of 100 nm/100 nm, (iii) Al nanoscale line array with L/S of 200 nm/200 nm, and (iv) SiO_2 nanoscale line array with L/S of 100 nm/100 nm. Scale bar = 5 μm.

deposition angle is critical and can affect the result of transfer. If vertical deposition (i.e., deposition angle of 0° with respect to the normal axis of the substrate plane) is used, the material is deposited on both the top and trench areas of the patterned HA film. This undesirable deposition result can be avoided by depositing the film at an oblique angle (i.e., nonzero deposition angle).

Moreover, the pattern spacing and shape can be controlled by adjusting the deposition thickness and angle (Figure S2). Finally, the designed nanostructures are transferred onto the textile, as shown in Figure 1a(ii). An image of the HA film with a Au line array having a line width of 200 nm and spacing of 200 nm (L/S of 200 nm/200 nm) is provided in the inset of Figure 1a(ii), with the corresponding SEM image shown in Figure 1c. The detailed transfer process of nanostructures from HA film to textile is shown in Figure 1a(iii). During the transfer process, it is important that the reaction proceeds simultaneously in the entire HA film area; otherwise, the film can be deformed and defects can be generated. For this reason, the film is placed on a wet textile substrate. Over the wet substrate, the HA film, which has a high water adsorption property owing to the abundant hydrophilic functional groups, swells and changes into a gel-like state. As dissolved HA is gel-like, it helps in maintaining the shape of the nanostructure. Water is continuously supplied around the film, and the dissolved HA solution is diluted and absorbed by the underlying wiper *via* capillary action, allowing the facile transfer of functional materials with micro/nanoscale patterns onto the textile substrate. During the final stage of the nTP-SP, it is presumed that the functional material patterns are adhered onto the textile by van der Waals forces. Figure 1d shows the textile surface having an arbitrary morphology without any

https://dx.doi.org/10.1021/acsnano.9b09082
ACS Nano 2020, 14, 2191−2201

nanostructures. When the HA film with nanostructures is partially dissolved by water, the metal nanostructures are attached onto the surface of the textile because of the adhesive force of the remaining HA. Owing to these characteristics, the functional material with a thickness of less than 100 nm is preserved without any extra adhesive layer, whereas the HA film with a thickness of ~20 μm is gradually dissolved by water. The SEM image including the functional material with partially dissolved HA film is displayed in Figure 1e. The SEM image in Figure 1f shows that most of the HA is dissolved and the metal nanostructures are suspended between the textile fibers. Figure S3 shows the nTP-SP process from the initial state when the nanostructures start to settle on the textile assisted by the gel-like HA film to the final result with no HA residue remaining due to the continuous water supply. At the beginning, the nanostructures are uniformly connected between the fibers by the existing HA. As water is supplied, HA is partially removed in the suspended area, and the remaining HA agglomerates because of the viscosity of HA. As a result, the nanopatterns of functional materials are also agglomerated on the suspended regions.

One notable advantage of HA compared with other water-soluble polymers such as poly(vinyl alcohol) (PVA) is that its dissolution rate is faster than that of PVA, which reacts slowly or rarely with water at room temperature. The solubility of PVA is very low below 70 °C.[47] In contrast, HA dissolves immediately upon contact with water at room temperature. Subsequently, a connection is formed between polymer chains, and the HA film swells and becomes viscoelastic. This is because HA has more hydrophilic groups and thus a superior adsorption property of water molecules (Figure S4a). PVA also reacts with water to form a cross-linked structure, which causes the volume to swell.[48] However, PVA, which has a slow reaction rate at room temperature, has different degrees of swelling in the same film. Therefore, while the lower surface in contact with the water swells slightly, the upper surface does not swell, and this difference causes the film to curl, thereby making it difficult to settle on the textile. A comparison between HA and PVA is provided in Figure S4.

To further prove the versatility of our proposed method, transfer of various nanopatterns (i.e., nanoscale line, dots, and mesh) and materials (i.e., Au, Ag, Al, Pd, and SiO_2) on the textile substrate was implemented.

Figure 2a shows the transfer results for various Au nanopatterns including line array (L/S of 200 nm/200 nm; Figure 2a(i)), dot array (hexagonal array with a diameter of 480 nm and pitch of 1000 nm; Figure 2a(ii)), and mesh structure that was created by transferring a line pattern (L/S of 200 nm/200 nm) twice (Figure 2a(iii)). To confirm the minimum line width and spacing that can be applied, Au line patterns having line widths of 50, 100, and 200 nm were transferred (Figure S5). The Au nanostructure was effectively transferred for all three line widths, indicating that stable transfer was possible regardless of the line width. However, as the line spacing narrowed, some line-to-line contact was created during the deposition process. The proposed method can be used to transfer various other materials, as shown in Figure 2b. Figure 2b(i) shows the result for the transfer of a Pd line array with L/S of 200 nm/200 nm. In addition, a pattern with L/S of 100 nm/100 and 200 nm/400 nm was transferred (Figure S6). Figure 2b(ii) shows the result for the transfer of a Ag line array with L/S of 100 nm/100 nm. Additionally, a line array with L/S of 200 nm/200 nm and a hole array with a diameter of 265 nm and pitch of 530 nm were successfully transferred (Figure S7). Figure 2b(iii) shows the transfer result of an Al line array with L/S of 200 nm/200 nm, and the transfer results with L/S of 100 nm/100 nm are provided in Figure S8. Figure 2b(iv) shows the transfer result of a SiO_2 line array with L/S of 100 nm/100 nm. SiO_2 was relatively well transferred for L/S of 100 nm/100 nm, while the line array pattern with L/S of 200 nm/200 nm exhibited broken parts on both the suspended region and the fiber surface (Figure S9). In this regard, the results differed slightly depending on the material. The ductility of the deposited material, cross-sectional area, and distance between fibers can affect the transfer quality. First, as mentioned above, when HA reacts with water, it swells and changes into a gel-like state. In this process, the ductility of the material deposited on HA can affect the transfer results. Au (ductility: 0.93) with high ductility showed the most stable result among all materials used. It was confirmed that the transfer result slightly deteriorated for different materials in the order of Pd (ductility: 0.8), Ag (ductility: 0.73), Al (ductility: 0.65), and SiO_2 (ductility: 0), which is the same as the order of their ductility. Additional factors affecting the transfer results are the cross-sectional area and the distance between the fibers. To verify this, the transfer results for the line pattern were modeled as a cable that had the same level of support on both sides and received a uniformly distributed load. The corresponding tensile force (T) can be defined as

$$T = \frac{wL^2}{8h}\sqrt{1 + \left(\frac{dy}{dx}\right)^2} \quad (1)$$

where w, h, and L are the distributed load per unit distance, deflection height at center, and distance between fibers, respectively. At the nanoscale, the effect of gravitational force due to the self-weight is negligible. Instead, surface tension applied to the line pattern is a dominant force during the transfer process. As depicted in eq 1, when the distance between the fibers is large, considerable tensile force is applied to the pattern. In this regard, when the tension is larger than the allowable value, the line pattern is likely to be broken in the suspended area. However, breakage by tension is a local occurrence, and there are sufficient connections to allow electric current to flow across the transferred metal pattern as a whole.

After the nTP-SP process, the presence of HA was analyzed using focused ion beam (FIB), SEM, and Fourier transform infrared (FTIR) spectroscopy, and the results are shown in Figure S10. Surface image analysis through SEM and cross-sectional and surface image analysis through FIB confirmed that no residue was present on the fibers except for the deposited material. For FTIR spectroscopy, a pristine textile that was not used for the transfer process was employed as a reference (Figure S10, blue spectrum). To determine the presence or absence of HA, a sample with the remaining HA that was removed by placing the wiper underneath the textile substrate (Figure S10, red spectrum) was compared with a sample with only the film placed on the textile substrate (Figure S10, black spectrum). HA has various functional groups, as shown in Figure S10a, but the O−H group exists only in HA in comparison to the functional groups in textiles. The spectrum of the sample using the wiper (Figure S10, red spectrum) shows that the O−H group almost disappears and no corresponding peak in the 3400−3650 cm^{-1} (O−H band

https://dx.doi.org/10.1021/acsnano.9b09082
ACS Nano 2020, 14, 2191−2201

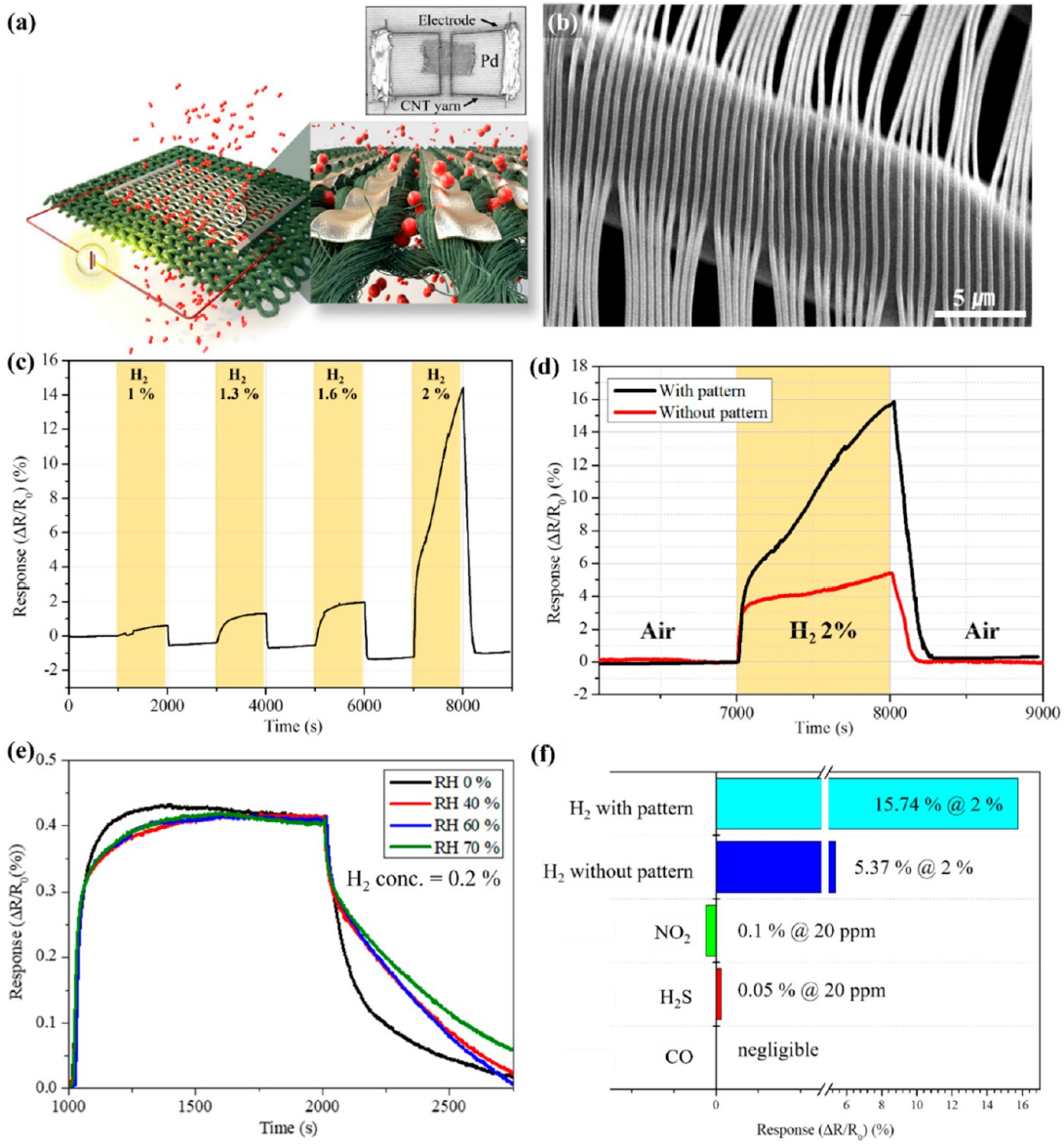

Figure 3. Application of the nTP-SP process to the fabrication of Pd nanostructure for hydrogen (H_2) gas sensing: (a) schematic of the H_2 sensor using a textile substrate (inset: optical image of the fabricated sensor); (b) SEM image of the nanostructure with L/S of 200 nm/200 nm fabricated on a fabric substrate; (c) response ($\Delta R/R_0$) of the fabricated device to H_2 gas; (d) comparison of responses between Pd nanopattern and film transferred onto the textile substrate; (e) H_2 response of the sensor under different relative humidity conditions (0−70%); (f) selectivity test for various gases (NO_2, H_2S, and CO).

position) region is observed. In addition, the spectral features are similar to those of the reference textile. This implies that the residual HA was removed by the wiper. Contrarily, the spectrum of the sample placed on the textile substrate without using the wiper (Figure S10, black spectrum) shows that a peak appears at the band position corresponding to the O−H group due to the remaining HA.[49] Through this analysis, it was confirmed that most of the remaining HA was removed through the capillary effect by placing the wiper under the substrate.

Next, the nTP-SP process was performed on different textile substrates, and the results are summarized in Figure S11. Conventional synthetic textiles typically contain polyester (PE) and/or spandex (SP), where spandex is a water-absorbing material. Therefore, it was possible to transfer the desired patterns and materials by dissolving the patterned HA film using water on these textile substrates. Similar results can be obtained for different textile substrates with the same components but with varying ratios between PE and SP. This process can also be applied to the textiles containing nylon (NY) and a clean paper containing cellulose, both of which are water-absorbing materials. However, textile consisting of only PE can absorb relatively less water, and therefore, more water has to be supplied during the transfer process to remove residual HA. Additionally, when the textile is made of materials that cannot effectively absorb water such as glass fiber, it is possible to transfer the pattern if the space exists between the fibers and water can pass through it. Although there is a slight difference in the patterning quality depending on the different types of substrates, the proposed method is applicable to a variety of textile substrates that can absorb or allow the passage of water.

Furthermore, nTP-SP was conducted to examine the effect of the line width, fiber array topology, and pattern type (Figure

https://dx.doi.org/10.1021/acsnano.9b09082
ACS Nano 2020, 14, 2191−2201

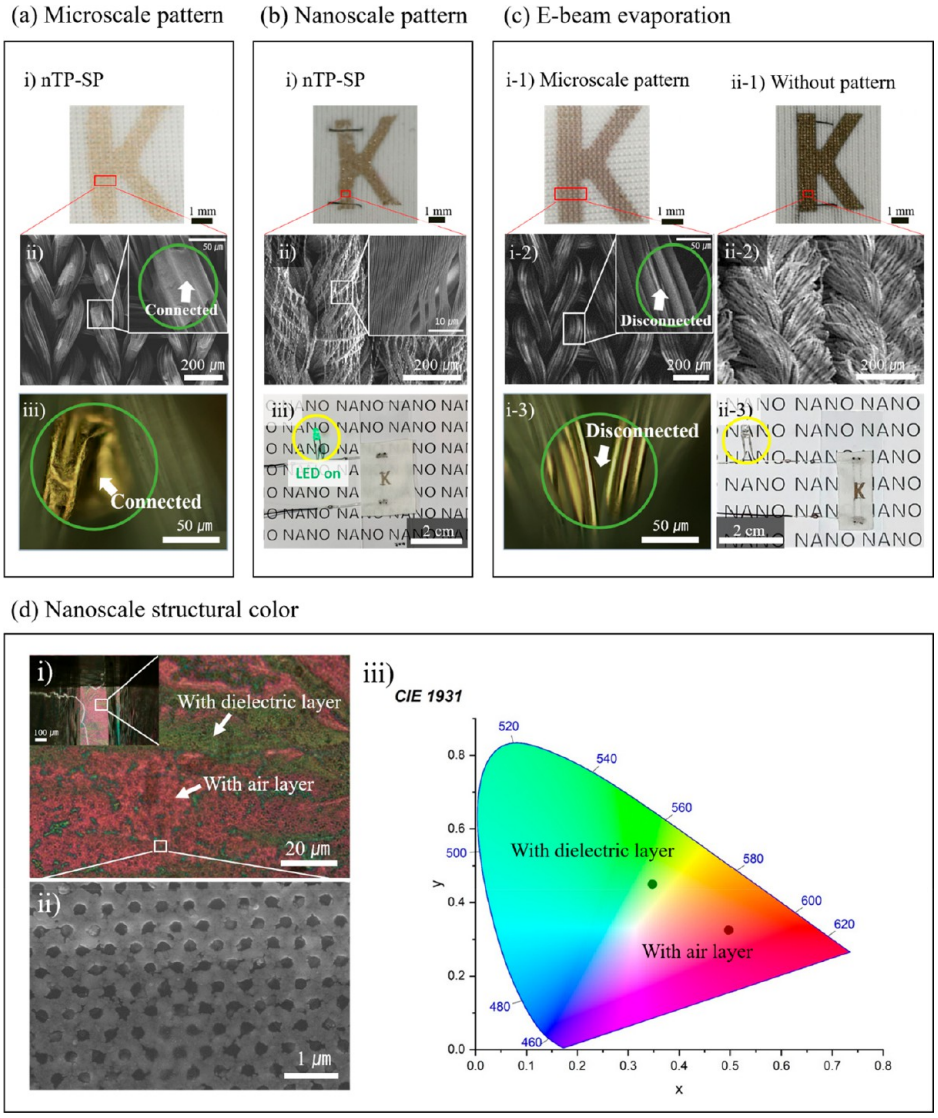

Figure 4. Application of the nTP-SP process to the fabrication of Au and Ag nanostructures and security patterns: (a) nTP-SP results using a microscale Au dot pattern with a diameter of 100 μm and a pitch of 150 μm, (ii) its SEM image, and (iii) its magnified optical microscopy image; (b) nTP-SP results using a nanoscale Au line pattern with L/S of 200 nm/200 nm, (ii) its SEM image, and (iii) verification of the electrical conduction through transferred patterns by LED operation; (c) results of direct Au e-beam evaporation (i) with microscale dot patterns and (ii) without patterns; (d) nanoscale structural color based on transferred Ag nanopatterns with a diameter of 265 nm and a pitch of 530 nm (i), its SEM image (ii), and FDTD simulation shown on the CIE 1931 coordinates (iii).

S12). Both microscale and nanoscale line patterns were well transferred onto the textile substrate, and since the same textile presented different arrangements on the front and rear sides, the obtained result was found to depend on the side of the textile employed. This demonstrates that, using the same textile and same nanopattern, a denser fiber arrangement was obtained on the rear side, and the distance between fibers was reduced, thereby resulting in more uniform pattern transfer than that on the front side. It can also be seen that the results differ depending on the relationship between the direction of transferred patterns and that of fibers. In addition, the pattern type was found to affect the transfer performance. More specifically, the hole pattern was more connected than the line pattern. This can be attributed to the fact that the line pattern is a one-dimensional pattern, while the hole pattern is a two-dimensional pattern with better connection between features. As such, the transfer results were found to vary depending on the pattern type, the arrangement of fibers, and the morphology of the textile substrate. It is therefore necessary to select an appropriate textile substrate and pattern for the effective transfer processes.

For practical applications in flexible and wearable devices, the mechanical stability of the fabricated pattern should be ensured. As such, electromechanical characterization tests were performed, including bending and rubbing tests. Figure S13 shows the results of the cyclic bending tests performed with a bending radius of 75−14 mm. More specifically, using a bending radius of 75 mm, we confirmed that the resistance fluctuated between 106 and 117% of the initial resistance. As the bending radius was decreased to 25, 18, and 14 mm, the maximum resistance reached up to 133, 260, and 550% of the initial resistance, respectively, and these results were repeatable. In addition, at the beginning of the bending cycle, the resistance change was relatively large; however, as the cycles were repeated, consistent results were obtained. This can be attributed to the ductility of the gold nanoline arrays.

https://dx.doi.org/10.1021/acsnano.9b09082
ACS Nano 2020, 14, 2191−2201

Although the initial resistance is high because the nanolines stretch and break, contact between the broken nanolines occurs as the bending is repeated (i.e., like a switch), and the resistance gradually decreases. It therefore takes time to initialize and stabilize the sample in the wearable device. We also conducted a rubbing test to determine the effect of shear forces. Figure S14 shows the results of the first, third, and fourth rubbing tests. The conductivity was measured after rubbing the sample with a finger to determine whether the resistance could increase by the rubbing forces. During the first rubbing test, many nanowires were broken, causing a large change in the conductivity. These results indicate that the shear forces could break the nanowires between the fibers, but breakage of the wires on the fibers was less significant. As such, the nanostructural color on the fiber will be maintained even though the electrical characteristics may change. If the fabricated devices are to be employed in practical applications, it is essential to ensure their mechanical stability against external forces by using an appropriate packaging.

It should be noted that our proposed method involves the use of a textile substrate and dissolution of the water-soluble polymer nanotemplate in water, and therefore, the patterning performance can be limited to a certain extent. For example, the functional film may not contact uniformly with the textile substrate due to the uneven topology of the substrate. In addition, when the dissolved solution flows through the nanopatterns, defects can occur. Furthermore, precise alignment is difficult due to the morphology of the textile substrate and the gel-like property of the dissolved template. However, these issues can be resolved by introducing the following methods: (1) optimization of the dissolution process by adjusting the concentration and thickness of the HA film, thereby reducing defects and promoting uniform contact with the textile substrate, or (2) alignment of the second layer prior to the complete dissolution of the HA of the first layer in the gel-like state to ensure more precise alignment.

In addition to the wetting property of the textile for the nTP-SP process, its excellent permeability is also important for various applications such as gas sensors. The textiles were made by twisting several yarns together, which generates high porosity. This property can be exploited for gas sensor applications, as shown in Figure 3a. In this study, a Pd-based H_2 gas sensor was fabricated using the nTP-SP process. An image of the fabricated gas sensor is shown in Figure 3a (inset). It was fabricated by transferring Pd nanopatterns with L/S of 200 nm/200 nm and stitching carbon nanotube (CNT) yarns for the electrical interconnection of Pd nanopatterns. The SEM image of the transferred pattern is shown in Figure 3b. The sensor produced a change in resistance depending on the H_2 concentration that varied from 1 to 2% and is presented in Figure 3c. To demonstrate the effect of the pattern, the response was measured for samples with and without patterns when injected with 2% H_2 gas. The response of the plain film was approximately 6%, while the sample with a nanopattern showed a response of 15% (Figure 3d and Figure S16a,b). This result verified the effect of nanostructures with a large surface area on the reaction with gas molecules. In addition, tests for the humidity effect on the sensor performance were conducted. Thus, gas sensing tests to 0.2% H_2 were conducted under various humidity conditions. As shown in Figure 3e, no major difference in the response was observed upon altering the humidity, while the response and recovery times were affected. It is speculated that water molecules adhered on the palladium surface may retard the adsorption of hydrogen molecules. Furthermore, selectivity tests were performed for different interfering gases (Figure 3f and Figure S16). According to Occupational Safety and Health Administration guidelines, permissible exposure limits are 5 ppm for NO_2, 10 ppm for H_2S, and 50 ppm for CO. The sensor showed a negligible response to CO gas up to 200 ppm. For 20 ppm of NO_2 gas, the sensor showed a negative response of 0.1%, while a response of 0.05% was observed for 20 ppm of H_2S. The H element contained in H_2S was partially decomposed and showed a small positive response.[50] By comparing the required detection ranges of these gases, it can be concluded that the sensor has a superior selectivity to H_2 relative to other interfering gases because of the selective reaction of Pd with H_2 to generate PdH_x. Based on these results, it was verified that the proposed method could be used to fabricate a gas sensor suitable for H_2 sensing.

In addition, the transferred pattern can be utilized as a security pattern with an anticounterfeiting function (Figure 4). The method is capable of transferring a pattern at the nanoscale as well as the microscale. To demonstrate the applicability of the security pattern, two approaches were used: (1) characters consisting of microscale or nanoscale patterns (Figure 4a and b) and (2) optical characteristics of nanostructures with localized surface plasmon resonance (LSPR) (Figure 4d). The nTP-SP results for letters consisting of microscale dot patterns show that thin films connect separate fibers (Figure 4a(ii) and (iii)). When a letter composed of nanoscale line patterns using the nTP-SP process is transferred, the connection between the fibers can also be confirmed, as presented in Figure 4b(ii). Figure 4b(iii) shows that the LED turns on when it is connected at both ends of the transferred letter due to the connection between the fibers *via* the transferred nanoscale line patterns. In contrast, the film is disconnected between the separate fibers if these are directly deposited by the e-beam evaporation process (Figure 4c(i) and (ii)). As a result, the LED connected to both ends of the letter does not turn on. In addition to an e-beam evaporation, sputtering deposition with a relatively better conformal deposition capability also exhibited no connection between fibers, as shown in Figure S17. From these results, it can be concluded that the authenticity of valuable products can be determined by electrical or optical measurement of the printed patterns.

Furthermore, nanoscale Ag hole patterns having a diameter of 265 nm and a pitch of 530 nm were fabricated on a textile substrate to generate LSPR, which affords a nanoscale structural color.[51] Optical microscopy and SEM images are shown in Figure 4d(i) and (ii). When the nanostructure is suspended between the fibers (i.e., on the air layer), it has a red-like color. When the nanostructures are on the fibers or if there is residual HA (i.e., on the dielectric layer), it has a greenish-yellow color. This shows a distinct color difference when compared with the result of transferring a patternless film having the same thickness (Figure S18). This experimental result is supported by the finite-difference time-domain (FDTD) numerical simulation. A hexagonal nanohole array structure made of Ag with a diameter of 265 nm and a pitch of 530 nm was simulated, as shown in Figure S18 (inset). As presented in Figure 4d(iii), reddish-magenta is the structural color for the Ag nanohole array suspended in the atmospheric layer and greenish-yellow is the structural color for the Ag nanohole array located on the polymer substrate. To provide a

https://dx.doi.org/10.1021/acsnano.9b09082
ACS Nano 2020, 14, 2191−2201

proof-of-concept demonstration, we altered the thickness of the Ag layer, the hole diameter, and the pitch between holes, as shown in Figure S18. From the experiment, it was found that, even for the same nanohole pattern, the color can differ (i.e., blue or red) depending on the thickness of the deposited Ag layer. Furthermore, despite the same thickness of the deposited Ag layer, a yellow color appears as the diameter and pitch are changed. The simulation results match well with the experimental data. From these numerical and experimental analyses, it can be confirmed that the Ag film on the textile substrate exhibits unique structural colors, which are different from the original Ag color, if it contains a periodic nanopattern array. Thus, it can be used to determine the authenticity of valuables by checking the unique structural colors originating from the particular nanostructures.

Moreover, a self-cleaning function of TiO_2 nanostructures was verified using our proposed method (Figure S19). The degree of natural decomposition of methylene blue solution (MB) under visible light was only ~10% after 40 min of exposure. On the other hand, the MB was decomposed by ~40% on the textile where the Ag/TiO_2 nanostructures were transferred. In this process, a Ag nanopattern was introduced to improve the light absorption due to LSPR to promote the photocatalytic activity of TiO_2. By this result, we have confirmed that not only the metal but also the nonmetal nanostructures can be well transferred onto textile substrate for enhanced surface functionality such as the self-cleaning effect. It is predicted that the self-cleaning function of TiO_2 nanostructures can be applied to textiles such as bacteria inactivation and environmental purification.[46]

CONCLUSIONS

In summary, a process for transferring nanopatterned functional materials onto a textile substrate using HA, a water-soluble polymer, has been proposed. This method is effective for textile substrates with high surface roughness and water absorption property. HA is dissolved in water to directly transfer metal or SiO_2 nanostructures, such that no additional adhesive layer is required. Using the proposed method, it was verified that various materials including noble metals (Au, Pd, Ag, and Al) and SiO_2 with different nanostructures such as lines, holes, and mesh patterns can be transferred onto the textile substrates. Since our proposed method involves the use of a textile substrate and a water-soluble process, limitations exist, including those associated with alignment and defects. However, these issues can be resolved by employing several parameter adjustments and additional procedures. The usefulness of this process to practical applications such as H_2 sensors using Pd nanoscale line patterns, security patterns using structural colors of nanoscale patterns, and the self-cleaning function by transferring TiO_2 nanostructures has been demonstrated. The proposed nanopatterning method can provide a facile route for the fabrication of various functional devices on textile or paper substrates, including sweat sensors, environmental monitoring devices, catalytic filters, and fabric supercapacitors.

EXPERIMENTAL SECTION

Fabrication of a Nanoscale Patterned Si Master. The Si master with nanoscale patterns was fabricated by KrF optical lithography and the reactive ion etching process. Then, the fabricated Si master was treated with trichloro(1*H*,1*H*,2*H*,2*H*-perfluorooctyl)-silane (Sigma-Aldrich, USA) to achieve good separation from the resin during the pattern replication process.

Replication of a Si Master to Polymer Film. A previously published[52,53] polymer mold fabrication process was used, and the details are provided in the Supporting Information (Figure S1). The UV-curable polyurethane acrylate resin (311-RM, Munuta Tech. Co., Ltd., Korea) was poured on the Si master to replicate the nanoscale pattern. The Si master with resin was covered with polyethylene terephthalate film. Pressure was applied to remove the trapped air and fill the pattern with resin using a roller. Finally, UV curing was performed twice for 90 s each.

Fabrication of HA Solution. To make a 1 wt % solution, HA powder (HA-TLM 20−40 (200−400 kDa), Bloomage Bio Technology Co., Ltd., China) was stirred with water as a solvent at 550 rpm at room temperature for 4 h.

Fabrication of HA Film with a Pattern. The polymer film replicated from the Si master was cut into 3 cm × 3 cm size and fixed on a Petri dish (diameter = 55 mm). Then, 1 wt % HA solution was poured over it. The Petri dish was placed in a vacuum chamber for 10 min to remove air bubbles caused by pouring. The sample was dried at 50 °C in a convection oven for 1 day.

Deposition of Functional Materials on Patterned HA Film. The functional materials were obliquely deposited on the patterned HA film by electron beam evaporation (Daeki Hi-Tech Co., Ltd., Korea) with a deposition angle of 60° at a rate of 1.5−2 Å/s under high vacuum (pressure of ~10^{-6} Torr).

Surface and Cross-Sectional Image Analysis. Field emission-scanning electron microscopy (Sirion, Thermo Fisher Scientific, Inc., USA) and FIB microscopy (Helios Nanolab, Thermo Fisher Scientific, Inc., USA) were used to obtain high-resolution surface and cross-sectional images.

FTIR Spectroscopy. An FTIR spectrometer (Nicolet iS50, Thermo Fisher Scientific, Inc., USA) was used to determine the presence of HA and HA residue in the samples.

Optical Image Analysis. An optical microscope (Eclipse LV 100, Nikon Instruments, Inc., USA) was used to visualize the morphologies and to evaluate the optical properties of the samples.

Bending Tests. Bending tests were performed using a linear stage. The real-time resistance was measured using a source meter (Keithley 2635B, Tektronix, Inc., USA). The tests were repeated 1000 times at 2−4 s/cycle for a bending radius range of 75−14 mm.

Gas Sensing Experiment. Gas sensing experiments were performed in a sealed chamber with a probe. The real-time resistance was measured through a source meter (Keithley 2635B, Tektronix, Inc., USA). Mass flow controllers (MFCs) were used to control the gas concentration and flow rate. The source meter and MFCs were controlled *via* the LabVIEW interface (the gas test setup is shown in Figure S15). The change in resistance during the test was measured by repeatedly flowing hydrogen gas and air at intervals of 1000 s. Selectivity tests were performed using carbon monoxide, nitrogen dioxide, and hydrogen sulfide.

Microscale/Nanoscale Security Pattern Experiment. The sample with a microscale security pattern involved a metal film deposited using a shadow mask, consisting of micropatterns with 100 μm holes and 150 μm pitch, on a HA film without any pattern. The sample with a nanoscale security pattern involved a metal film deposited using a letter-shaped shadow mask on a HA film, with nanoscale line patterns of L/S = 200 nm/200 nm. As a control group, the same metal was e-beam evaporated directly on the textile through a shadow mask. In addition, a sample with an LSPR effect, one of the characteristics of the nanostructure, was fabricated. A nanoscale Ag hole pattern array with a diameter of 265 nm and a pitch of 530 nm was transferred on a glass fiber mat.

Numerical Simulation for Nanoscale Structural Color. FDTD Solution (Lumerical Inc., Canada), an FDTD simulation software, was used to compute the nanostructural color. A perfectly matched layer was placed on the top and bottom to avoid interference caused by reflection, and the periodic boundary condition was specified by dividing the mesh at intervals of 3 nm. A Ag nanostructure comprising a hexagonal hole array with a diameter of

https://dx.doi.org/10.1021/acsnano.9b09082
ACS Nano 2020, 14, 2191−2201

265 nm and a pitch of 530 nm was designed, and the inside of the hole was designated as air. Optical transmission was simulated by increasing the thickness of the polymer layer from 0 to 450 nm under the nanostructure. At this time, the simulation values were measured by placing the designed structure and monitor under the source at intervals of 200 nm. The simulated electromagnetic wave was converted to frequency using a fast Fourier transform. The obtained FDTD frequency results were plotted in CIE 1931 coordinates using a chromaticity diagram of Origin.

Photocatalysis Experiment. Ag with a 50 nm thickness was obliquely deposited on the patterned HA film having L/S = 100 nm/100 nm with a deposition angle of 45°, followed by TiO_2 with the same thickness and deposition angle. The sample with transferred Ag/TiO_2 nanostructure was placed in a beaker containing 6 mL of 10 ppm methylene blue (MB) solution and exposed to a visible light source illuminator (LAX-C100, Asahi spectra USA Inc., USA). A UV−vis spectrometer (Lambda 750, PerkinElmer Inc., USA) with UV quartz cuvette was employed to measure the degree of MB decomposition every 10 min.

ASSOCIATED CONTENT

Supporting Information

The Supporting Information is available free of charge at https://pubs.acs.org/doi/10.1021/acsnano.9b09082.

Additional characterization of the nanopattern transfer process. Figures S1−S19 and Table S1 providing the summary of solvent-assisted transfer methods; the nanotransfer process; the results according to the deposition angles; the results of the transfer process *via* SEM image; the comparison between HA and PVA; the SEM images of functional materials (Au, Pd, Ag, Al, and SiO_2) transfer for various nanopatterns; the residual HA validation *via* FTIR, FIB, and SEM; the results for different substrate type; bending and rubbing test results; gas sensing experimental setup and raw data of gas sensing; nanoscale structural colors for different thicknesses of Ag and SiO_2 obtained using FDTD simulation; normalized absorbance of MB after photocatalysis and SEM image (PDF)

AUTHOR INFORMATION

Corresponding Authors

Jun-Ho Jeong − *Nano-Convergence Mechanical Systems Research Division, Korea Institute of Machinery and Materials (KIMM), Daejeon 34103, South Korea; Department of Nano-Mechatronics, University of Science and Technology (UST), Daejeon 34113, South Korea;* orcid.org/0000-0003-0671-0225; Email: jhjeong@kimm.ac.kr

Inkyu Park − *Department of Mechanical Engineering, Korea Advanced Institute of Science and Technology (KAIST), Daejeon 34141, South Korea;* orcid.org/0000-0001-5761-7739; Email: inkyu@kaist.ac.kr

Authors

Jiwoo Ko − *Department of Mechanical Engineering, Korea Advanced Institute of Science and Technology (KAIST), Daejeon 34141, South Korea; Nano-Convergence Mechanical Systems Research Division, Korea Institute of Machinery and Materials (KIMM), Daejeon 34103, South Korea*

Zhi-Jun Zhao − *Nano-Convergence Mechanical Systems Research Division, Korea Institute of Machinery and Materials (KIMM), Daejeon 34103, South Korea*

Soon Hyoung Hwang − *Nano-Convergence Mechanical Systems Research Division, Korea Institute of Machinery and Materials (KIMM), Daejeon 34103, South Korea*

Hyeok-Joong Kang − *Nano-Convergence Mechanical Systems Research Division, Korea Institute of Machinery and Materials (KIMM), Daejeon 34103, South Korea*

Junseong Ahn − *Department of Mechanical Engineering, Korea Advanced Institute of Science and Technology (KAIST), Daejeon 34141, South Korea; Nano-Convergence Mechanical Systems Research Division, Korea Institute of Machinery and Materials (KIMM), Daejeon 34103, South Korea*

Sohee Jeon − *Nano-Convergence Mechanical Systems Research Division, Korea Institute of Machinery and Materials (KIMM), Daejeon 34103, South Korea*

Moonjeong Bok − *Nano-Convergence Mechanical Systems Research Division, Korea Institute of Machinery and Materials (KIMM), Daejeon 34103, South Korea*

Yongrok Jeong − *Nano-Convergence Mechanical Systems Research Division, Korea Institute of Machinery and Materials (KIMM), Daejeon 34103, South Korea*

Kyungnam Kang − *Department of Mechanical Engineering, Korea Advanced Institute of Science and Technology (KAIST), Daejeon 34141, South Korea*

Incheol Cho − *Department of Mechanical Engineering, Korea Advanced Institute of Science and Technology (KAIST), Daejeon 34141, South Korea*

Complete contact information is available at: https://pubs.acs.org/10.1021/acsnano.9b09082

Author Contributions

The manuscript was written through contributions of all authors. J.K. performed all experiments, analyzed the data, and wrote the paper. J.K., Z.-J.Z., S.H.H., H.-J.K., J.A., M.B., and Y.J. discussed the fabrication and results of nanotransfer printing using water-soluble polymer. J.K., Y.J., K.K., and I.C. discussed the results of the gas sensor. J.K., Z.-J.Z., S.H.H., H.-J.K., and S.J. discussed the results of the security pattern and nanoscale structural color. J.-H.J. and I.P. led the overall direction of the project.

Notes

The authors declare no competing financial interest.

ACKNOWLEDGMENTS

This work was supported by the National Research Foundation of Korea (NRF) grant funded by the Korea government (MSIT; No. 2018R1A2B2004910) and by the Center for Advanced Meta-Materials (CAMM) funded by the Ministry of Science, ICT, and Future Planning, Korea, through the Global Frontier Project (CAMM-No. 2014M3A6B3063707).

REFERENCES

(1) Yetisen, A. K.; Qu, H.; Manbachi, A.; Butt, H.; Dokmeci, M. R.; Hinestroza, J. P.; Skorobogatiy, M.; Khademhosseini, A.; Yun, S. H. Nanotechnology in Textiles. *ACS Nano* **2016**, *10*, 3042−3068.

(2) Sandt, J. D.; Moudio, M.; Clark, J. K.; Hardin, J.; Argenti, C.; Carty, M.; Lewis, J. A.; Kolle, M. Stretchable Optomechanical Fiber Sensors for Pressure Determination in Compressive Medical Textiles. *Adv. Healthcare Mater.* **2018**, *7*, No. 1800293.

(3) Liu, M.; Pu, X.; Jiang, C.; Liu, T.; Huang, X.; Chen, L.; Du, C.; Sun, J.; Hu, W.; Wang, Z. L. Large-Area All-Textile Pressure Sensors for Monitoring Human Motion and Physiological Signals. *Adv. Mater.* **2017**, *29*, 1703700.

(4) Lin, Z.; Yang, J.; Li, X.; Wu, Y.; Wei, W.; Liu, J.; Chen, J.; Yang, J. Large-Scale and Washable Smart Textiles Based on Triboelectric Nanogenerator Arrays for Self-Powered Sleeping Monitoring. *Adv. Funct. Mater.* **2018**, *28*, 1704112.
(5) Cao, R.; Pu, X.; Du, X.; Yang, W.; Wang, J.; Guo, H.; Zhao, S.; Yuan, Z.; Zhang, C.; Li, C.; Wang, Z. L. Screen-Printed Washable Electronic Textiles as Self-Powered Touch/Gesture Tribo-Sensors for Intelligent Human−Machine Interaction. *ACS Nano* **2018**, *12*, 5190−5196.
(6) Torres Alonso, E.; Rodrigues, D. P.; Khetani, M.; Shin, D.-W.; De Sanctis, A.; Joulie, H.; de Schrijver, I.; Baldycheva, A.; Alves, H.; Neves, A. I. S.; Russo, S.; Craciun, M. F. Graphene Electronic Fibres with Touch-Sensing and Light-Emitting Functionalities for Smart Textiles. *npj Flexible Electron.* **2018**, *2*, 25.
(7) Paradiso, R.; Loriga, G.; Taccini, N. A Wearable Health Care System Based on Knitted Integrated Sensors. *IEEE Trans. Inf. Technol. Biomed.* **2005**, *9*, 337−344.
(8) Rein, M.; Favrod, V. D.; Hou, C.; Khudiyev, T.; Stolyarov, A.; Cox, J.; Chung, C.-C.; Chhav, C.; Ellis, M.; Joannopoulos, J.; Fink, Y. Diode Fibres for Fabric-Based Optical Communications. *Nature* **2018**, *560*, 214−218.
(9) Witt, J.; Narbonneau, F.; Schukar, M.; Krebber, K.; De Jonckheere, J.; Jeanne, M.; Kinet, D.; Paquet, B.; Depre, A.; D'Angelo, L. T.; Thiel, T.; Logier, R. Medical Textiles with Embedded Fiber Optic Sensors for Monitoring of Respiratory Movement. *IEEE Sens. J.* **2012**, *12*, 246−254.
(10) Grillet, A.; Kinet, D.; Witt, J.; Schukar, M.; Krebber, K.; Pirotte, F.; Depre, A. Optical Fiber Sensors Embedded into Medical Textiles for Healthcare Monitoring. *IEEE Sens. J.* **2008**, *8*, 1215−1222.
(11) Lee, J.; Kwon, H.; Seo, J.; Shin, S.; Koo, J. H.; Pang, C.; Son, S.; Kim, J. H.; Jang, Y. H.; Kim, D. E.; Lee, T. Conductive Fiber-Based Ultrasensitive Textile Pressure Sensor for Wearable Electronics. *Adv. Mater.* **2015**, *27*, 2433−2439.
(12) Collins, G. E.; Buckley, L. J. Conductive Polymer-Coated Fabrics for Chemical Sensing. *Synth. Met.* **1996**, *78*, 93−101.
(13) Kwon, O. S.; Park, E.; Kweon, O. Y.; Park, S. J.; Jang, J. Novel Flexible Chemical Gas Sensor Based on Poly(3,4-Ethylenedioxythiophene) Nanotube Membrane. *Talanta* **2010**, *82*, 1338−1343.
(14) Hong, K. H.; Oh, K. W.; Kang, T. J. Polyaniline−Nylon 6 Composite Fabric for Ammonia Gas Sensor. *J. Appl. Polym. Sci.* **2004**, *92*, 37−42.
(15) Low, K.; Horner, C. B.; Li, C.; Ico, G.; Bosze, W.; Myung, N. V.; Nam, J. Composition-Dependent Sensing Mechanism of Electrospun Conductive Polymer Composite Nanofibers. *Sens. Actuators, B* **2015**, *207*, 235−242.
(16) Chuang, M.-C.; Windmiller, J. R.; Santhosh, P.; Ramirez, G. V.; Galik, M.; Chou, T. Y.; Wang, J. Textile-Based Electrochemical Sensing: Effect of Fabric Substrate and Detection of Nitroaromatic Explosives. *Electroanalysis* **2010**, *22*, 2511−2518.
(17) Coyle, S.; Lau, K.-T.; Moyna, N.; O'Gorman, D.; Diamond, D.; Di Francesco, F.; Costanzo, D.; Salvo, P.; Trivella, M. G.; De Rossi, D. E.; Taccini, N.; Paradiso, R.; Porchet, J.-A.; Ridolfi, A.; Luprano, J.; Chuzel, C.; Lanier, T.; Revol-Cavalier, F.; Schoumacker, S.; Mourier, V.; et al. BIOTEX—Biosensing Textiles for Personalised Healthcare Management. *IEEE Trans. Inf. Technol. Biomed.* **2010**, *14*, 364−370.
(18) Weremczuk, J.; Tarapata, G.; Jachowicz, R. Humidity Sensor Printed on Textile with Use of Ink-Jet Technology. *Procedia Eng.* **2012**, *47*, 1366−1369.
(19) Devaux, E.; Aubry, C.; Campagne, C.; Rochery, M. PLA/Carbon Nanotubes Multifilament Yarns for Relative Humidity Textile Sensor. *J. Eng. Fibers Fabr.* **2011**, *6*, 13−24.
(20) Zhang, Z.; Cui, L.; Shi, X.; Tian, X.; Wang, D.; Gu, C.; Chen, E.; Cheng, X.; Xu, Y.; Hu, Y.; Zhang, J.; Zhou, L.; Fong, H. H.; Ma, P.; Jiang, G.; Sun, X.; Zhang, B.; Peng, H. Textile Display for Electronic and Brain-Interfaced Communications. *Adv. Mater.* **2018**, *30*, 1800323.
(21) Pu, X.; Li, L.; Liu, M.; Jiang, C.; Du, C.; Zhao, Z.; Hu, W.; Wang, Z. L. Wearable Self-Charging Power Textile Based on Flexible Yarn Supercapacitors and Fabric Nanogenerators. *Adv. Mater.* **2016**, *28*, 98−105.
(22) Seung, W.; Gupta, M. K.; Lee, K. Y.; Shin, K. S.; Lee, J. H.; Kim, T. Y.; Kim, S.; Lin, J.; Kim, J. H.; Kim, S. W. Nanopatterned Textile-Based Wearable Triboelectric Nanogenerator. *ACS Nano* **2015**, *9*, 3501−3509.
(23) Jung, S.; Lee, J.; Hyeon, T.; Lee, M.; Kim, D. H. Fabric-Based Integrated Energy Devices for Wearable Activity Monitors. *Adv. Mater.* **2014**, *26*, 6329−6334.
(24) Yu, A.; Pu, X.; Wen, R.; Liu, M.; Zhou, T.; Zhang, K.; Zhang, Y.; Zhai, J.; Hu, W.; Wang, Z. L. Core−Shell-Yarn-Based Triboelectric Nanogenerator Textiles as Power Cloths. *ACS Nano* **2017**, *11*, 12764−12771.
(25) Dong, K.; Wang, Y. C.; Deng, J.; Dai, Y.; Zhang, S. L.; Zou, H.; Gu, B.; Sun, B.; Wang, Z. L. A Highly Stretchable and Washable All-Yarn-Based Self-Charging Knitting Power Textile Composed of Fiber Triboelectric Nanogenerators and Supercapacitors. *ACS Nano* **2017**, *11*, 9490−9499.
(26) Pu, X.; Song, W.; Liu, M.; Sun, C.; Du, C.; Jiang, C.; Huang, X.; Zou, D.; Hu, W.; Wang, Z. L. Wearable Power-Textiles by Integrating Fabric Triboelectric Nanogenerators and Fiber-Shaped Dye-Sensitized Solar Cells. *Adv. Energy Mater.* **2016**, *6*, 1601048.
(27) Zhang, N.; Chen, J.; Huang, Y.; Guo, W.; Yang, J.; Du, J.; Fan, X.; Tao, C. A Wearable All-Solid Photovoltaic Textile. *Adv. Mater.* **2016**, *28*, 263−269.
(28) Chen, J.; Huang, Y.; Zhang, N.; Zou, H.; Liu, R.; Tao, C.; Fan, X.; Wang, Z. L. Micro-Cable Structured Textile for Simultaneously Harvesting Solar and Mechanical Energy. *Nat. Energy* **2016**, *1*, 16138.
(29) Kim, S. J.; We, J. H.; Cho, B. J. A Wearable Thermoelectric Generator Fabricated on a Glass Fabric. *Energy Environ. Sci.* **2014**, *7*, 1959−1965.
(30) Zhao, Z.; Yan, C.; Liu, Z.; Fu, X.; Peng, L. M.; Hu, Y.; Zheng, Z. Machine-Washable Textile Triboelectric Nanogenerators for Effective Human Respiratory Monitoring through Loom Weaving of Metallic Yarns. *Adv. Mater.* **2016**, *28*, 10267−10274.
(31) Rothmaier, M.; Luong, M. H.; Clemens, F. Textile Pressure Sensor Made of Flexible Plastic Optical Fibers. *Sensors* **2008**, *8*, 4318−4329.
(32) El-Sherif, M. A.; Yuan, J.; MacDiarmid, A. Fiber Optic Sensors and Smart Fabrics. *J. Intell. Mater. Syst. Struct.* **2000**, *11*, 407−414.
(33) Kinkeldei, T.; Zysset, C.; Cherenack, K.; Troester, G. Development and Evaluation of Temperature Sensors for Textile Integration. In *2009 IEEE Sensors*, Christchurch, New Zealand, Oct 25−28, 2009, 1580−1583.
(34) Lee, S.; Shin, S.; Lee, S.; Seo, J.; Lee, J.; Son, S.; Cho, H. J.; Algadi, H.; Al-Sayari, S.; Kim, D. E.; Lee, T. Ag Nanowire Reinforced Highly Stretchable Conductive Fibers for Wearable Electronics. *Adv. Funct. Mater.* **2015**, *25*, 3114−3121.
(35) Frutiger, A.; Muth, J. T.; Vogt, D. M.; Mengüç, Y.; Campo, A.; Valentine, A. D.; Walsh, C. J.; Lewis, J. A. Capacitive Soft Strain Sensors *via* Multicore−Shell Fiber Printing. *Adv. Mater.* **2015**, *27*, 2440−2446.
(36) Han, J. T.; Choi, S.; Jang, J. I.; Seol, S. K.; Woo, J. S.; Jeong, H. J.; Jeong, S. Y.; Baeg, K. J.; Lee, G. W. Rearrangement of 1D Conducting Nanomaterials towards Highly Electrically Conducting Nanocomposite Fibres for Electronic Textiles. *Sci. Rep.* **2015**, *5*, 9300.
(37) Yong, S.; Owen, J.; Beeby, S. Solid-State Supercapacitor Fabricated in a Single Woven Textile Layer for E-Textiles Applications. *Adv. Eng. Mater.* **2018**, *20*, 1700860.
(38) Shim, B. S.; Chen, W.; Doty, C.; Xu, C.; Kotov, N. A. Smart Electronic Yarns and Wearable Fabrics for Human Biomonitoring Made by Carbon Nanotube Coating with Polyelectrolytes. *Nano Lett.* **2008**, *8*, 4151−4157.
(39) Abu Hatab, N. A.; Oran, J. M.; Sepaniak, M. J. Surface-Enhanced Raman Spectroscopy Substrates Created *via* Electron Beam Lithography and Nanotransfer Printing. *ACS Nano* **2008**, *2*, 377−385.
(40) Chanda, D.; Shigeta, K.; Gupta, S.; Cain, T.; Carlson, A.; Mihi, A.; Rogers, J. A. Large-Area Flexible 3D Optical Negative Index

https://dx.doi.org/10.1021/acsnano.9b09082
ACS Nano 2020, 14, 2191−2201

Metamaterial Formed by Nanotransfer Printing. *Nat. Nanotechnol.* **2011**, *6*, 402−407.
(41) Park, K. S.; Baek, J.; Park, Y.; Lee, L.; Lee, Y. E. K.; Kang, Y.; Sung, M. M. Inkjet-Assisted Nanotransfer Printing for Large-Scale Integrated Nanopatterns of Various Single-Crystal Organic Materials. *Adv. Mater.* **2016**, *28*, 2874−2880.
(42) Xue, M.; Ma, X.; Xie, Z.; Duan, L.; Jiang, Y.; Zhang, M.; Cao, T. Fabrication of Gold-Directed Conducting Polymer Nanoarrays for High-Performance Gas Sensor. *Chem. - Asian J.* **2010**, *5*, 2266−2270.
(43) Bareiß, M.; Hochmeister, A.; Jegert, G.; Koblmüller, G.; Zschieschang, U.; Klauk, H.; Lugli, P. Energy Harvesting Using Nano Antenna Array. In *the 11th IEEE Int. Conf. Nanotechnol.*, Portland, OR, Aug 15−18, 2011, 218−221.
(44) Kim, T. Y.; Kim, S. K.; Kim, S.-W. Application of Ferroelectric Materials for Improving Output Power of Energy Harvesters. *Nano Converg.* **2018**, *5*, 30−45.
(45) Kim, T. H.; Cho, K. S.; Lee, E. K.; Lee, S. J.; Chae, J.; Kim, J. W.; Choi, B. L. Full-Colour Quantum Dot Displays Fabricated by Transfer Printing. *Nat. Photonics* **2011**, *5*, 176−182.
(46) Eom, H.; Jung, J. Y.; Shin, Y.; Kim, S.; Choi, J. H.; Lee, E.; Jeong, J. H.; Park, I. Strong Localized Surface Plasmon Resonance Effects of Ag/TiO_2 Core−Shell Nanowire Arrays in UV and Visible Light for Photocatalytic Activity. *Nanoscale* **2014**, *6*, 226−234.
(47) Finch, C. A. *Polyvinyl Alcohol: Developments*; Wiley: Chichester, U.K., 1992.
(48) Urushizaki, F.; Yamaguchi, H.; Nakamura, K.; Numajiri, S.; Sugibayashi, K.; Morimoto, Y. Swelling and Mechanical Properties of Poly(Vinyl Alcohol) Hydrogels. *Int. J. Pharm.* **1990**, *58*, 135−142.
(49) Ahire, J. J.; Robertson, D.; Neveling, D. P.; Van Reenen, A. J.; Dicks, L. M. T. Hyaluronic Acid-Coated Poly(D,L-Lactide) (PDLLA) Nanofibers Prepared by Electrospinning and Coating. *RSC Adv.* **2016**, *6*, 34791−34796.
(50) Cho, M.; Yun, J.; Kwon, D.; Kim, K.; Park, I. High-Sensitivity and Low-Power Flexible Schottky Hydrogen Sensor Based on Silicon Nanomembrane. *ACS Appl. Mater. Interfaces* **2018**, *10*, 12870−12877.
(51) Lee, T.; Jang, J.; Jeong, H.; Rho, J. Plasmonic- and Dielectric-Based Structural Coloring: From Fundamentals to Practical Applications. *Nano Converg.* **2018**, *5*, 1−21.
(52) Zhao, Z. J.; Shin, S. H.; Choi, D. G.; Park, S. H.; Jeong, J. H. Nanowelding: Shape-Controlled 3D Periodic Metal Nanostructures Fabricated *via* Nanowelding. *Small* **2018**, *14*, 1703102.
(53) Hwang, S. H.; Jeon, S.; Kim, M. J.; Choi, D. G.; Choi, J. H.; Jung, J. Y.; Young, J. R. Covalent Bonding-Assisted Nanotransfer Lithography for the Fabrication of Plasmonic Nano-Optical Elements. *Nanoscale* **2017**, *9*, 14335−14346.

https://dx.doi.org/10.1021/acsnano.9b09082
ACS Nano 2020, 14, 2191−2201